Measurement of inverse pion photoproduction at energies spanning the $N(1440)$ resonance

A. Shafi,[1] S. Prakhov,[2] I. I. Strakovsky,[1] W. J. Briscoe,[1,*] B. M. K. Nefkens,[2] C. E. Allgower,[3,†] R. A. Arndt,[1] V. Bekrenev,[4] C. Bennhold,[1] M. Clajus,[2] J. R. Comfort,[5] K. Craig,[5] D. Grosnick,[6] D. Isenhower,[7] N. Knecht,[8] D. D. Koetke,[6] A. Kulbardis,[4] N. Kozlenko,[4] S. Kruglov,[4] G. Lolos,[8] I. Lopatin,[4] D. M. Manley,[9] R. Manweiler,[6] A. Marušić,[2,‡] S. McDonald,[2,§] J. Olmsted,[9,†] Z. Papandreou,[8] D. Peaslee,[10] N. Phaisangittisakul,[2] J. W. Price,[2] A. F. Ramirez,[5] M. Sadler,[7] H. Spinka,[3] T. D. S. Stanislaus,[6] A. Starostin,[2,4] H. M. Staudenmaier,[11] I. Supek,[12] W. B. Tippens,[2,‖] and R. L. Workman[1]
(The Crystal Ball Collaboration)
[1]*The George Washington University, Washington, DC 20052-0001, USA*
[2]*University of California Los Angeles, Los Angeles, California 90095-1547, USA*
[3]*Argonne National Laboratory, Argonne, Ilinois 60439-4815, USA*
[4]*Petersburg Nuclear Physics Institute, Gatchina, Russia 188300*
[5]*Arizona State University, Tempe, Arizona 85287-1504, USA*
[6]*Valparaiso University, Valparaiso, Indiana 46383-6493, USA*
[7]*Abilene Christian University, Abilene, Texas 79699-7963, USA*
[8]*University of Regina, Saskatchewan, Canada S4S OA2*
[9]*Kent State University, Kent, Ohio 44242-0001, USA*
[10]*University of Maryland, College Park, Maryland 20742-4111, USA*
[11]*Universität Karlsruhe, Karlsruhe, Germany 76128*
[12]*Rudjer Boskovic Institute, Zagreb, Croatia 10002*
(Received 6 May 2004; published 21 September 2004)

Differential cross sections for the process $\pi^- p \to \gamma n$ have been measured at Brookhaven National Laboratory's Alternating Gradient Synchrotron with the Crystal Ball multiphoton spectrometer. Measurements were made at 18 pion momenta from 238 to 748 MeV/c, corresponding to E_γ for the inverse reaction from 285 to 769 MeV. The data have been used to evaluate the γn multipoles in the vicinity of the $N(1440)$ resonance. We compare our data and multipoles to previous determinations.

DOI: 10.1103/PhysRevC.70.035204 PACS number(s): 25.20.Lj, 13.60.Le, 25.40.Lw

I. INTRODUCTION

The study of the light baryon resonances, in particular the determination of their electromagnetic couplings, is undergoing a resurgence driven by a stream of new, high-precision data emanating from experimental programs at modern photon facilities. The main properties of the $\Delta(1232)$ resonance, the mass, pole value, mass splittings, width, and branching ratio for different decay modes are now reasonably well known. In addition, there are data on the deformation from a spherical shape, the E_2/M_1 ratio, and the magnitude and sign of the magnetic dipole moment of the $\Delta^{++}(1232)$. In comparison with this, the properties of the lightest N^* resonance, the $N(1440)$, are much more uncertain. The Crystal Ball baryon-resonance program at Brookhaven National Laboratory's (BNL) Alternating Gradient Synchrotron (AGS) is providing much needed data on the $N(1440)$ resonance via new, precision measurements of γ, π^0, and $2\pi^0$ production in $\pi^- p$ interactions. These data will permit new, state-of-the-art coupled-channel analyses to be performed. This paper presents results of the $\pi^- p \to \gamma n$ measurements.

The $N(1440)$, often called the Roper resonance, has the quantum numbers of the nucleon ground state, $I, J^P = \frac{1}{2}, \frac{1}{2}^+$. The lightness of the mass is somewhat of a surprise, as several models, including the relativized quark model for baryons [1], imply that the lowest mass states are the $N(1520)\frac{3}{2}^-$ and $N(1535)\frac{1}{2}^-$. A better understanding of the Roper resonance is particularly important as its radiative decay width is larger than predicted. This has led to a number of theoretical speculations concerning its underlying structure. The Roper resonance could be a radial excitation of the nucleon [1] or a hybrid state consisting of three quarks and a gluon [2]. In an algebraic framework for the description of baryons, Bijker, Iachello, and Leviatan studied a collective stringlike model to obtain masses and electromagnetic couplings [3]. Modern lattice-gauge calculations with constrained curve-fitting techniques are also now being used to study the Roper resonance [4]. Recently, it was conjectured that the Roper resonance might be a pentaquark state and a member of an antidecuplet [5]. The classification of the Roper resonance as an antidecuplet was already proposed by Lovelace [6] back in 1965. Donnachie [7] suggested a simple test for this hypothesis. By using *U-spin* conservation one can easily show that the radiative decay of the charged Roper resonance is not allowed, $N(1440) \nrightarrow \gamma p$; however, the radiative decay of the neutral

*Electronic address: briscoe@gwu.edu
†Present address: Midwest Proton Radiotherapy Institute, 2425 N. Milo Sampson Lane, Bloomington, IN 47408.
‡Present address: Collider-Accelerator Dept., Brookhaven National Laboratory, Upton, NY 11973.
§Present address: TRIUMF, 4004 Wesbrook Mall, Vancouver, B.C., Canada V6T 2A3.
‖Present address: Nuclear Physics Division, Department of Energy, 19901 Germantown Road, Germantown, MD 20874-1290.

TABLE I. $N(1440)$ resonance couplings from a Breit-Wigner fit to the recent GW-SAID-2002 single-energy solution [GW02] [8], the previous solution SM95 [VPI95] [9], the analysis of Crawford and Morton [CM83] [10], Crawford [CR01] [11], Drechsel *et al.* [MAID98] [12], [MAID03] [13], the coupled-channels fit of Niboh and Manley [KSU97] [14], GW-CC coupled channels calculation [BENN03] [15], the average of Feuster and Mosel [FM99] [16], the average from the Particle Data Group [PDG02] [17], and quark model predictions by Capstick [CAP92] [1]. Units are $(\mathrm{GeV})^{-1/2}\times 10^{-3}$. None of these include the results of this paper.

Resonance state	Reference	$A^p_{1/2}$	$A^n_{1/2}$
$W_{\mathrm{Roper}}\approx 1440$ MeV	GW02	-67 ± 2	47 ± 5
$\Gamma_\pi/\Gamma\approx 0.65$	VPI95	-63 ± 5	45 ± 15
$\Gamma\approx 350$ MeV	CM83	-69 ± 18	56 ± 15
	CR01	-88	
	MAID98	-71	60
	MAID03	-77	52
	KSU97	-81 ± 6	65 ± 12
	BENN03	-81	59
	FM99	-74	51
	PDG02	-65 ± 4	40 ± 10
	CAP92	4	-6

Roper resonance is allowed, $N(1440)\rightarrow\gamma n$ The extracted γn and γp decay amplitudes are not small (see Table I), which does not support the conjecture [5] that the Roper resonance is a member of an antidecuplet.

The radiative decay width of the charged Roper resonance is readily extracted from π^+ and π^0 photoproduction on a proton. The radiative decay width of the neutral state may be extracted from π^- or π^0 photoproduction off a neutron, which involves a bound neutron target (typically the deuteron) and requires the use of a model-dependent nuclear correction. As a result, our knowledge of neutral resonance decays is less precise than of the charged ones. An example is given by the Roper resonance photon-decay amplitudes listed in Table I. The PDG listings assign a 25% uncertainty to the Roper resonance γn amplitude, while a 6% uncertainty is assigned to the γp amplitude. The associated photoproduction multipoles are plotted in Fig. 1. Both the γp and γn multipoles have sizable uncertainties at the energies that correspond to the formation of the broad Roper resonance.

The existing photoproduction database contains a large set of $\gamma n\rightarrow\pi^- p$ differential cross sections. Many of these are old bremsstrahlung measurements with limited angular coverage. In several cases, the systematic uncertainties have not been quoted. An accurate treatment of final-state interaction (FSI) effects for the pion photoproduction reactions on the deuteron, $\gamma d\rightarrow\pi^- pp$ and $\gamma d\rightarrow\pi^0 np$, is essential for the extraction of the spin-flip part of the photoproduction amplitudes. In addition, the photon decay amplitudes for the $N(1440)$ resonance, $A^p_{1/2}$ and $A^n_{1/2}$, are similar in magnitude and opposite in sign, suppressing the impulse-approximation contribution to the $\gamma d\rightarrow\pi^- pp$ reaction. As a result, diagrams involving meson rescattering give a significant contribution to the full amplitude.

The radiative decay of the neutral Roper resonance can also be obtained from the measurements of the inverse π^- photoproduction reaction

$$\pi^- p\rightarrow\gamma n, \tag{1}$$

which we will call REX for Radiative EXchange. This process is free from complications associated with the deuteron target. However, the disadvantage of using this reaction is the high background from the 5 to 500 times larger cross section for

$$\pi^- p\rightarrow\pi^0 n\rightarrow\gamma\gamma n, \tag{2}$$

called CEX for Charge EXchange. The Crystal Ball (CB) multiphoton spectrometer allows us to make a good measurement of the REX reaction with the reliable subtraction of the CEX-reaction background. These considerations motivated the measurement of inverse pion photoproduction cross sections (E913) [18] by the CB Collaboration at the BNL-AGS.

An extensive set of measurements over the energy range associated with the Roper resonance is essential to validate the existing multipole analyses from which the radiative widths are extracted, and to test the consistency of data that have been obtained with a deuterium target. We report here on the determination of the differential cross section for

$$\gamma n\rightarrow\pi^- p \tag{3}$$

from a measurement of the inverse reaction at 18 incident π^- momenta from 238 to 748 MeV/c. This range corresponds to E_γ from 285 to 769 MeV for the inverse process, covering the region most sensitive to the $N(1440)$ resonance; it effectively doubles the database for the π^- photoproduction reaction. In Sec. V, we discuss our analysis of the differential cross sections. The results of this experiment are presented in Sec. VI. We summarize our findings in Sec. VII.

II. EXPERIMENTAL SETUP

Our measurements of $\pi^- p\rightarrow\gamma n$ were made at BNL with the CB detector, which was installed in the AGS C6 beam

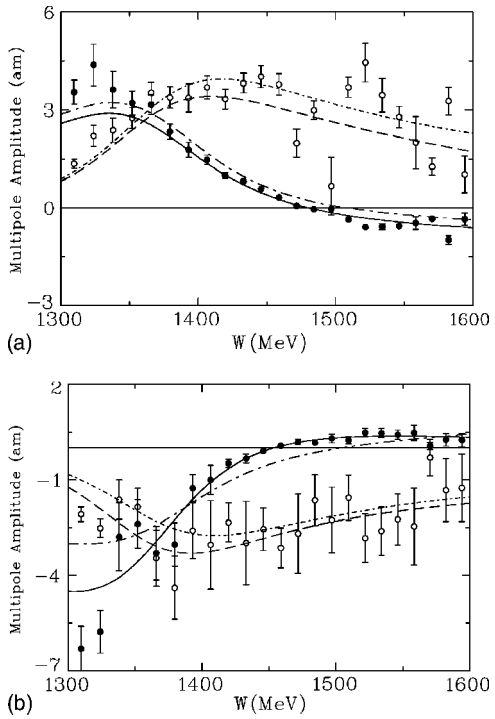

FIG. 1. $M_{1^-}^{1/2}$ multipoles in attometers (1 am$=10^{-18}$ m). Solid (dashed) curves give the real (imaginary) parts of amplitudes corresponding to the GW SM02 solution [8]. The real (imaginary) parts of GW single-energy solutions are plotted as filled (open) circles. The MAID solution [13] is plotted with long dashed-dotted (real part) and short dashed-dotted (imaginary part) lines. Plotted are the multipole amplitudes (a) ${}_pM_{1^-}^{1/2}$ and (b) ${}_nM_{1^-}^{1/2}$. The subscript $p(n)$ denotes a proton (neutron) target.

line. The CB consists of 672 NaI(Tl) crystals, each shaped like a truncated triangular pyramid. The crystals are optically isolated from their neighbors and arranged in two hemispheres with an entrance and exit tunnel for the beam and a spherical cavity in the center for the target. The CB covers 93% of 4π steradians.

The experiment was performed with a momentum-analyzed beam of negative pions, incident on a 10-cm-long liquid hydrogen (LH_2) target located in the center of the CB. The beam spread σ_p/p at the CB target was about 1%. The uncertainty in the mean momentum of the beam spectrum at the target center was 2–3 MeV/c.

The pulse height in each crystal was measured using a separate ADC. For registering timing information, we used a TDC on every minor triangle, which is a group of nine neighboring crystals. The typical energy resolution for electromagnetic showers in the CB was $\Delta E/E = 0.020/[E(\mathrm{GeV})]^{0.36}$. Showers were measured with a resolution in θ, the polar angle with respect to the beam axis, of $\sigma_\theta = 2° - 3°$ for photon energies in the range 50–500 MeV, assuming that the photons were produced in the center of the CB. The resolution in azimuthal angle ϕ is $\sigma_\theta/\sin\theta$.

The CB event trigger required a beam trigger in coincidence with a neutral event trigger, which included the requirement that the total energy deposited in the CB crystals exceeded a certain threshold. The beam trigger was a coincidence between three scintillation counters located in the beam line upstream of the CB. The neutral event trigger required that the CB event trigger signals were in anticoincidence with signals from a barrel of scintillation counters surrounding the target.

A more detailed description of the CB detector and the data analyses can be found in Refs. [18–21].

III. DATA ANALYSIS

To select candidates for the $\pi^- p \to \gamma n$ reaction, we used the neutral 1- and 2-cluster events, where we assumed that one of the clusters was due to a photon electromagnetic shower in the CB. A "cluster" is defined to be a group of neighboring crystals in which energy is deposited from a single-photon electromagnetic shower. The software threshold of the cluster energy was 14 MeV. For a 1-cluster event, the missing particle was assumed to be the neutron. For 2-cluster events, one of the clusters was assumed to come from a neutron interaction in the CB. The efficiency of the CB for neutrons has been found in a separate test to vary from 0 to 30% depending on the energy of the neutron [22]. In this experiment we used a lower cluster threshold (14 MeV) than in the test run (20 MeV) which increased our maximum neutron detection efficiency to 45%.

Since the REX cross section is small, the handling of the background is important. There are two kinds of background that must be subtracted from the $\pi^- p \to \gamma n$ event sample. The principal background comes from the CEX reaction, when one of the two photons from π^0 decay is not detected in the CB. Note that the total cross section for the CEX reaction is about two orders of magnitude larger than for the REX reaction [8,23]. The effect of this background process was estimated by determining the probability for Monte Carlo simulated CEX events to be misidentified as $\pi^- p \to \gamma n$ candidates. The input needed for the simulation of this background is the $\pi^- p \to \pi^0 n$ differential cross section that we have measured at each beam momentum in the same experiment. The fraction of events that are due to the CEX background depends mainly on the ratio of the production rates for the two processes. In the range of energies and angles reported in this paper, this fraction varies from 27% at our lowest momentum, 238 MeV/c, to 59% at our highest momentum, 748 MeV/c.

Other sources of background are due to processes that are not pion interactions in the liquid hydrogen of the target. The main contributions to this background are from beam pions that decayed or scattered before reaching the target, or interacted in the material surrounding the target. This background was investigated in runs taken with an empty target. The fraction of events that are due to the so-called "empty-target" background is of the order of a few percent, except at some extreme back angles.

All 1- and 2-cluster events were subjected to a kinematic fit to test the hypothesis of process (1), while all 2- and 3-cluster events were tested for the hypothesis of process (2). The kinematic fit has four main constraints (4-C) based on energy and 3-momentum conservation. The hypothesis for the CEX reaction has a fifth constraint that requires the invariant mass of the two photons to be the known π^0-meson

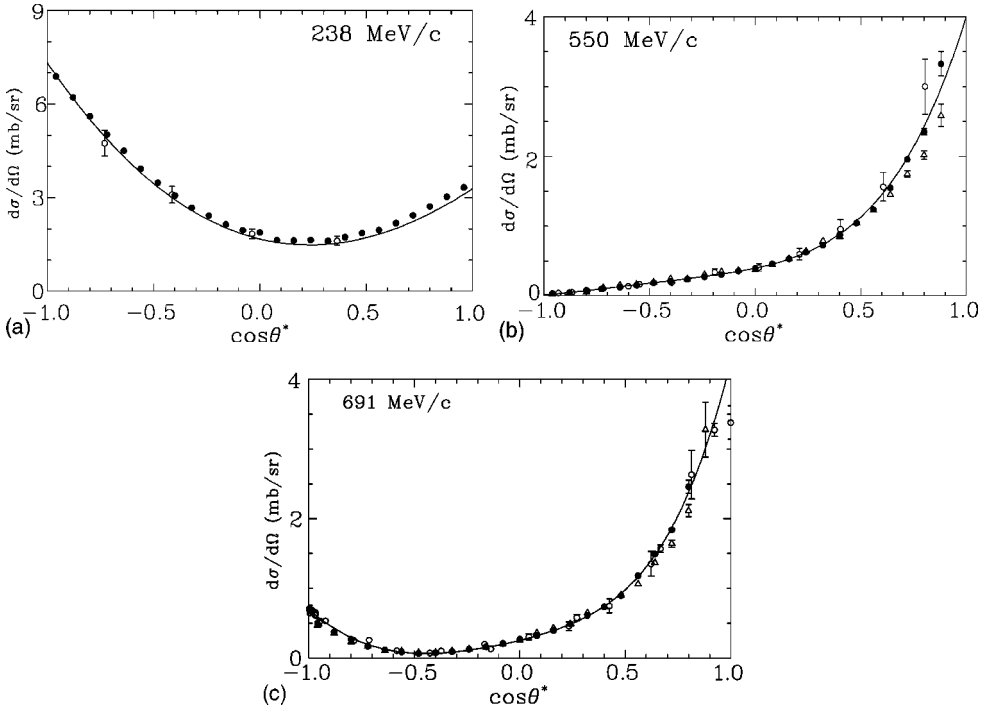

FIG. 2. The differential cross section for $\pi^- p \to \pi^0 n$ at an incident π^- momentum of (a) 238 MeV/c, (b) 550 MeV/c, and (c) 691 MeV/c. The LH_2 data (filled circles) at 550 and 691 MeV/c are normalized to the central part of the CH_2 spectra (open triangles). Solid lines show the GW SAID FA02 predictions [23]. Previous measurements [27] are shown as open circles.

mass. The measured parameters in the kinematic fit included five for the beam particle (momentum, angles θ_x and θ_y, and position coordinates x and y in the target) and three for each photon cluster (energy, angles θ and ϕ).

When the missing particle was the neutron, its energy and two angles were free parameters in the fit. For the neutron detected in the CB, the neutron angles were used as the measured parameters. In the case of the CEX reaction, the z coordinate of the primary vertex was a free parameter in the kinematic fit. Since the effective number of constraints is reduced by the number of free parameters of the fit, for the CEX reaction we have a 1-C (3-C) fit for 2-cluster (3-cluster) events. For the 1-cluster REX events we could not use the z coordinate of the vertex as a free parameter in the fit because the effective number of constraints would have been zero. To overcome this problem, the z coordinate was considered to be a "measured" parameter in the fit, with the mean equal to the center of the target and the variance one-third of the target thickness. For the 1-cluster events, we had a 1-C fit. The 2-cluster REX events have the neutron detected in the CB and thus the z coordinate can be a free parameter in a 2-C fit.

The kinematic fit pulls for the beam, photon, and neutron variables were adjusted to be in good agreement with ideal kinematical conditions with a normal distribution with mean value zero and variance 1. Some deviation occurs only for events with large cluster multiplicity, where some clusters overlap. While applying cuts on the confidence level of the kinematic fit, it is important to have good agreement between the probability distributions for the real and MC data. Such agreement has been illustrated in our earlier CB publications [20,21].

The confidence level (CL) of the kinematic fit was used to select the REX candidates. The 1-cluster events that satisfied the hypothesis above the 10% CL (i.e., with a probability greater than 10%) were accepted as $\pi^- p \to \gamma n$ candidates. The selection of 2-cluster REX events was performed in two steps. In the first step, the neutron information was used in the fit. This was necessary to suppress the large background from the CEX reaction. Those events that satisfied the hypothesis above the 1% CL proceeded to the second step in which the neutron information was omitted from the fit, and the event was treated in the same way as the 1-cluster case. Since the kinematic fit output is used for further analysis, this approach allows the 1- and 2-cluster events to have the same resolution for the photon production angle. In further analysis, we considered only the sum of 1- and 2-cluster events. This summation cancels problems associated with the small difference between the real and simulated events in the neutron response in the CB.

To select the CEX reaction events detected in the CB, we applied just a 2% CL criterion to hypothesis (2) for 2- and 3-cluster events. Similar to the $\pi^- p \to \gamma n$ selection, we added the 2- and 3-cluster events together. The only background that had to be subtracted was the empty-target one. The typical fraction of events due to this background was about 5%.

A Monte Carlo (MC) simulation of reaction (1) was performed for each momentum according to the phase-space distribution (i.e., with isotropic production angular distribution). The CEX reaction was simulated twice, once according to phase-space and once according to the shape of the differential cross sections that were determined in this experiment for each momentum. The simulation was made for every momentum by using the experimental beam-trigger events as

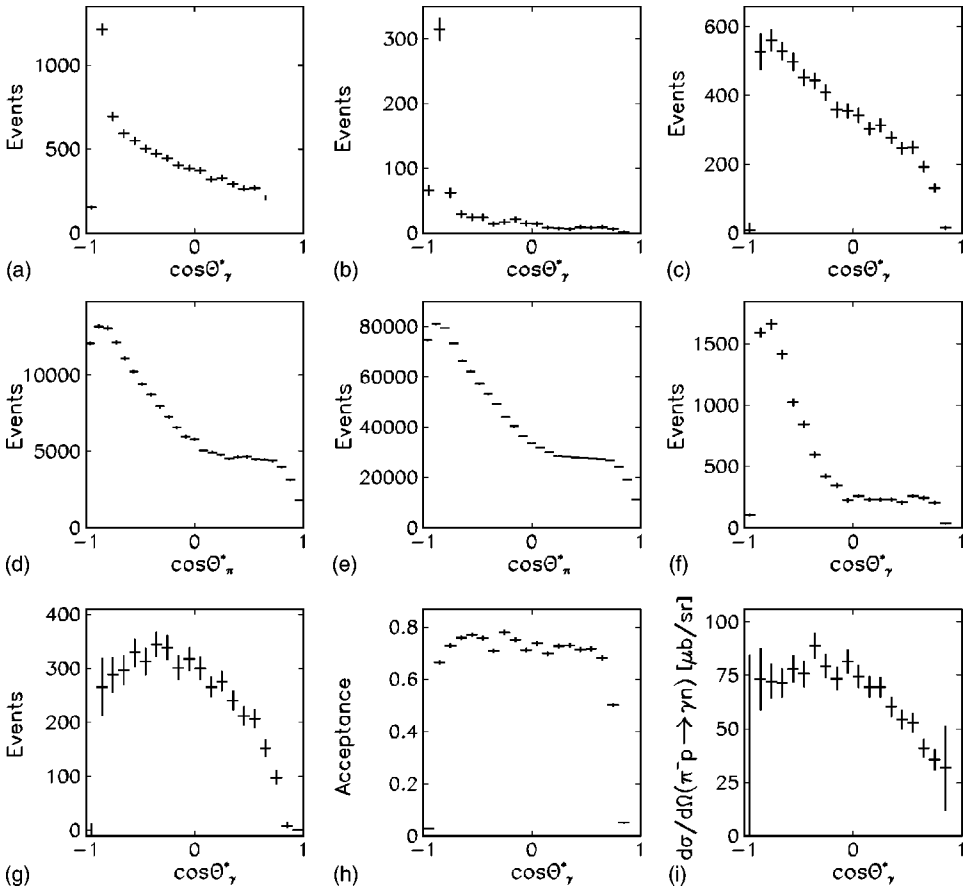

FIG. 3. The c.m. cos θ^* distributions for the production angle of the photon from $\pi^- p \to \gamma n$ and the π^0 from $\pi^- p \to \pi^0 n$ at $p_{\pi^-} = 238$ MeV/c: (a) the experimental candidates for $\pi^- p \to \gamma n$; (b) the empty-target events selected as $\pi^- p \to \gamma n$; (c) the REX candidates after the empty-target background subtraction; (d) the experimental CEX events; (e) the MC simulation for CEX events; (f) the CEX MC-simulation events misidentified as REX; (g) the REX events after both the empty-target and the CEX-background subtractions; (h) acceptance for $\pi^- p \to \gamma n$; and (i) the differential cross section for $\pi^- p \to \gamma n$.

input for pion-beam distributions. The MC events were then propagated through a full GEANT (version 3.21) [24] simulation of the CB detector, folded with the CB resolutions and trigger conditions, and analyzed in the same way as the experimental data.

The average detection efficiency for $\pi^- p \to \gamma n$ events generated according to phase space varied between 57% and 61% depending on the beam momentum and other experimental conditions. The values are slightly less than the geometrical acceptance of the CB for REX. The losses due to the exit hole in the CB are aggravated by the forward boost of the final-state photon in the laboratory system. Photon interactions in the beam pipe and in the barrel of scintillation counters surrounding the target also contribute to the loss of events. According to the simulation, the average probability for a photon not to pass the neutral trigger is about 6%. Finally, some decrease in the acceptance occurs due to the selection cuts used for the background suppression.

IV. THE NUMBER OF EFFECTIVE BEAM PIONS AND TARGET PROTONS

In addition to the determination of the number of initially produced REX and CEX events, the cross-section calculation needs the total number of beam pions, N_{π^-}, incident on the target and the effective number of hydrogen atoms in the target. The LH_2 target has a cylindrical shape along the beam direction and has hemispherical endcaps. The maximum target thickness along the beam axis is 10.57 cm. The hemisphere radius is 7.62 cm. The effective hydrogen density for the LH_2 conditions calculated in units of (mb cm)$^{-1}$ is $\rho^{\mathrm{Eff}}_{\mathrm{LH}_2} = 4.248 \times 10^{-5}$. The effective number of hydrogen atoms is $N^{\mathrm{Eff}}_{\mathrm{LH}_2} = \rho^{\mathrm{Eff}}_{\mathrm{LH}_2} \times l^{\mathrm{Eff}}_{\mathrm{LH}_2}$, where $l^{\mathrm{Eff}}_{\mathrm{LH}_2}$ is the effective thickness of the LH_2 target for the π^- beam passing through the entire target. This effective thickness was determined by a MC simulation, where the real beam-trigger events were used for calculating the average path length through the target. Taking into account the spatial distribution of the beam at different momenta, the effective number of hydrogen atoms in the LH_2 target is $N^{\mathrm{Eff}}_{\mathrm{LH}_2} = (4.05 \pm 0.08) \times 10^{-4}$ mb^{-1}.

The calculation of N_{π^-} involves several corrections that take into account the scattering and the decay of pions, and also the contamination of the pion beams by muons and electrons [25]. The decay and scattering of the beam pions were taken into account by simulation. The real beam-trigger events were used as input for this simulation. The trajectory information for the beam particles was measured by the drift chambers located in the beam line. For beam momenta below 350 MeV/c, the beam contamination by muons and electrons was measured by time-of-flight (TOF). There are several measurements of the CEX reaction in this energy range; a comparison of our CEX results with the existing data showed good agreement [26]. At all momenta, the electron contamination was also investigated by using a Čerenkov counter located in the beam downstream of the CB. However, our CEX results based on the Čerenkov counter information fell below the existing data. Since we relied entirely on the Čerenkov counter above 350 MeV/c, another

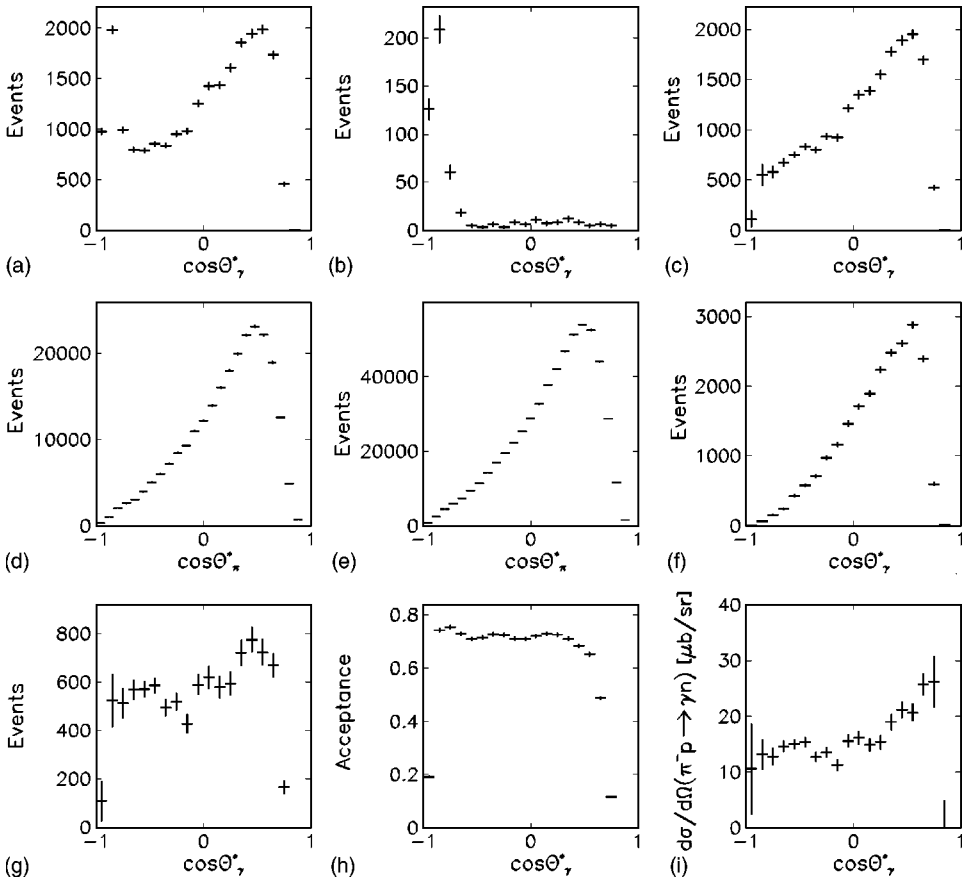

FIG. 4. Same as Fig. 3 but for $p_{\pi^-}=550$ MeV/c.

normalization method was used in our analysis.

The normalization of all LH_2 data sets with beam momenta above 350 MeV/c was made by remeasuring the CEX reaction with solid CH_2 targets. For the CH_2 measurements, the beam control was optimized to diminish uncertainties in the number of pions incident on the target. In Fig. 2(a), we show our LH_2 results for the CEX reaction at $p_{\pi^-}=238$ MeV/c. These results are obtained by using the beam information taken with the LH_2 target. In Figs. 2(b) and 2(c), we illustrate the normalization of the LH_2 data at $p_{\pi^-}=550$ and 691 MeV/c to the corresponding CH_2 spectra. To exclude the effect of low acceptance in the forward angles, we used only the angular region $\cos\theta^*_{\pi^0}<0.6$ for the normalization. More details about the beam normalization of the LH_2 data can be found in Ref. [21]. In Fig. 2 we also show the corresponding SAID [23] FA02 partial-wave analysis (PWA) of the existing data.

V. DETERMINATION OF THE $\pi^-p\to\gamma n$ DIFFERENTIAL CROSS SECTIONS

Figure 3 illustrates our procedure for determining the differential cross section of reaction (1) for our lowest beam momentum, 238 MeV/c. Each distribution in the figure is shown as a function of $\cos\theta^*$, where θ^* is the angle between the photon (or π^0) direction and the beam direction in the π^-p center-of-mass (c.m.) system. In Fig. 3(a), one can see the experimental distribution for all events selected as $\pi^-p\to\gamma n$ candidates. The empty-target background distribution is shown in Fig. 3(b). It can be seen that the largest contamination occurs at backward angles due to the decay of pions in the beam. The distribution remaining after the empty-target background subtraction is shown in Fig. 3(c). The subtraction of this background was made with a weight equal to the ratio of the number of incident pions for the full and the empty targets, respectively. This ratio varies from 2 to 5 depending on the relative beam on target of the full- and empty-target runs at each momentum. In Fig. 3(d), we show the experimental distribution of the events selected as the CEX reaction after the empty-target background subtraction. In Fig. 3(e), one can see the CEX distribution reconstructed for 2×10^6 $\pi^-p\to\pi^0n$ events simulated according to our differential cross section obtained for this reaction at the given momentum. The CEX background in the $\pi^-p\to\gamma n$ events is shown in Fig. 3(f). It was obtained from the simulated CEX events that survived the selection criteria for reaction (1). This background looks somewhat similar to the CEX distribution itself; however, the average probability for the CEX events to be misidentified as $\pi^-p\to\gamma n$ is about 0.8%. The $\cos\theta^*_\gamma$ distribution remaining after both the empty-target and the CEX background subtractions is shown in Fig. 3(g). The CEX background subtraction was made with a weight equal to the ratio of the CEX events reconstructed from the data and from the MC simulation. The acceptance for the $\pi^-p\to\gamma n$ reaction at $p_{\pi^-}=238$ MeV/c is shown in Fig. 3(h). This acceptance is about 75% for the central angles and drops in the forward and backward direction. Finally, the resulting differential cross section of reaction (1) at $p_{\pi^-}=238$ MeV/c is shown in Fig. 3(i) in units of μb/sr. To

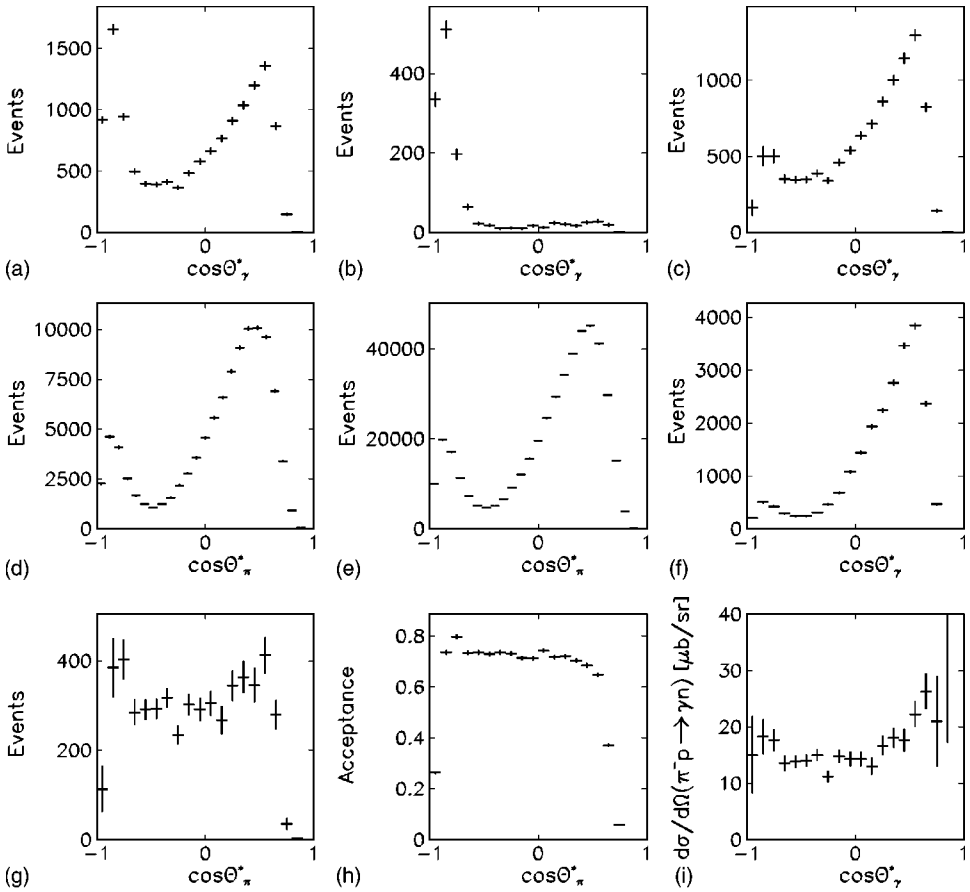

FIG. 5. Same as Fig. 3 but for $p_{\pi^-}=691$ MeV/c.

TABLE II. Differential cross section for $\gamma n \to \pi^- p$ (in μb/sr) as a function of center-of mass scattering angle and pion laboratory momentum (top row of header), and photon energy (bottom row of header). The quoted uncertainties are statistical and include the angle-dependent uncertainties due to the subtraction process and acceptance corrections. The total overall systematic uncertainty is about 5%. These are described in the text.

$\cos\theta^*_\pi$	238±3 MeV/c 285±3 MeV	271±3 MeV/c 313±3 MeV	298±3 MeV/c 338±3 MeV	322±3 MeV/c 359±3 MeV	355±4 MeV/c 390±4 MeV	373±4 MeV/c 407±4 MeV
−0.85	25.5±5.6	29.9±5.2	15.9±3.9	17.5±3.8	8.5±2.8	13.0±1.9
−0.75	25.2±3.1	29.2±3.1	18.3±2.4	14.9±2.3	10.1±1.8	8.9±1.0
−0.65	24.9±2.6	28.8±2.8	23.4±2.2	19.5±2.0	11.4±1.5	10.3±0.8
−0.55	27.2±2.3	28.3±2.6	23.2±2.0	15.8±1.8	12.0±1.4	10.2±0.7
−0.45	26.4±2.2	24.4±2.4	23.4±1.9	17.7±1.7	12.9±1.4	9.6±0.7
−0.35	31.0±2.2	30.5±2.3	19.7±1.8	17.9±1.8	11.1±1.3	9.9±0.6
−0.25	27.7±1.9	27.4±2.1	21.1±1.7	17.8±1.7	10.4±1.3	9.3±0.6
−0.15	25.6±2.0	23.8±2.0	21.0±1.6	17.0±1.5	12.6±1.4	11.1±0.6
−0.05	28.4±2.0	25.9±2.0	24.4±1.7	14.4±1.5	12.3±1.3	10.4±0.7
0.05	25.9±1.9	26.5±1.9	24.7±1.7	17.4±1.6	12.1±1.4	11.7±0.7
0.15	24.3±1.8	28.1±2.1	23.4±1.7	19.9±1.6	13.5±1.5	11.7±0.8
0.25	24.2±1.7	23.1±2.0	23.2±1.7	17.1±1.7	11.8±1.5	11.6±0.9
0.35	21.0±1.6	22.5±1.9	19.6±1.6	20.9±1.8	15.4±1.7	12.0±0.9
0.45	18.9±1.6	19.5±1.8	20.6±1.8	17.1±1.8	14.6±1.7	13.7±1.1
0.55	18.4±1.6	17.6±1.9	19.4±1.7	16.8±1.8	15.1±1.9	13.4±1.2
0.65	14.3±1.5	15.0±1.8	15.6±1.9	16.3±2.0	14.1±2.1	14.2±1.4
0.75	12.4±1.7	15.1±2.3	18.3±2.6	21.4±2.8	15.7±2.8	11.9±1.7

TABLE III. Continuation of Table II.

$\cos\theta_\pi^*$	404±4 MeV/c 436±4 MeV	472±5 MeV/c 501±5 MeV	550±5 MeV/c 576±5 MeV	656±6 MeV/c 679±6 MeV	668±6 MeV/c 691±6 MeV	678±6 MeV/c 700±6 MeV
−0.85	7.3±1.2	10.6±1.4	6.0±1.3	6.2±0.9	8.2±1.1	4.9±1.4
−0.75	7.1±0.6	5.7±0.9	5.8±0.7	6.4±0.6	7.2±0.7	7.2±0.8
−0.65	7.2±0.6	6.0±0.7	6.6±0.5	6.2±0.4	6.4±0.5	6.4±0.6
−0.55	7.8±0.6	6.4±0.6	6.8±0.4	6.5±0.3	5.8±0.5	6.4±0.5
−0.45	8.1±0.5	5.2±0.6	7.0±0.4	6.8±0.3	6.4±0.4	6.2±0.5
−0.35	7.5±0.5	6.4±0.6	5.8±0.5	5.6±0.4	6.9±0.5	6.4±0.5
−0.25	8.1±0.6	6.7±0.6	6.1±0.5	6.0±0.4	6.3±0.5	5.9±0.5
−0.15	7.8±0.6	5.3±0.7	5.1±0.6	6.1±0.6	6.4±0.6	6.5±0.6
−0.05	8.9±0.6	7.5±0.8	7.1±0.6	7.2±0.5	7.3±0.7	7.8±0.6
0.05	9.9±0.7	8.4±0.9	7.3±0.7	7.0±0.6	7.4±0.7	7.6±0.7
0.15	10.3±0.8	8.4±0.9	6.8±0.7	6.7±0.7	7.1±0.8	7.3±0.8
0.25	9.9±0.8	8.2±1.0	7.0±0.8	8.0±0.7	8.8±0.9	8.8±0.9
0.35	11.2±0.9	8.6±1.1	8.6±0.9	8.9±0.9	8.4±1.0	10.2±1.1
0.45	11.2±1.1	10.3±1.2	9.6±1.0	9.2±1.0	10.4±1.2	9.4±1.2
0.55	12.2±1.2	9.4±1.4	9.4±1.1	10.2±1.2	10.1±1.3	10.5±1.4
0.65	12.2±1.3	11.4±1.5	11.7±1.3	12.6±1.4	9.2±1.7	10.1±1.7
0.75	11.9±1.8	15.2±2.2	11.9±2.3	11.5±2.5	13.5±3.5	12.3±3.2

calculate the acceptance-corrected $\cos\theta_\gamma^*$ spectrum in these units, the number of events in a particular bin of the spectrum was multiplied by the factor $1000/(2\pi\times N_{\pi^-}\times N_{\mathrm{LH}_2}^{\mathrm{Eff}}\times\Delta\cos\theta_\gamma^*)$, where $\Delta\cos\theta_\gamma^*$ is the bin width. The uncertainties in all distributions shown in Fig. 3 are statistical only.

The same procedure was carried out at each of our 18 beam momenta. To illustrate the determination of differential cross sections at higher momenta, we show in Figs. 4 and 5 similar distributions for $p_{\pi^-}=550$ and 691 MeV/c. Note that increasing the beam momentum results in an increased probability for the CEX events to be misidentified as $\pi^-p\to\gamma n$; at $p_{\pi^-}=550$ and 691 MeV/c it is about 5%.

The main sources of experimental uncertainty are (i) the background subtraction, (ii) the acceptance correction, and (iii) the normalization procedure.

The uncertainty in the background subtraction has two components: the subtraction of CEX events that pass the REX event selection and the beam-related background. The

TABLE IV. Continuation of Table II.

$\cos\theta_\pi^*$	691±6 MeV/c 713±6 MeV	704±7 MeV/c 726±7 MeV	719±7 MeV/c 740±7 MeV	727±7 MeV 748±7 MeV	733±6 MeV 754±6 MeV	748±7 MeV 769±7 MeV
−0.85	8.6±1.7	7.7±0.9	9.4±1.4	6.5±1.2	7.7±1.9	4.5±1.4
−0.75	8.3±1.0	8.7±0.6	6.9±0.9	6.5±0.8	3.9±1.3	5.6±0.9
−0.65	6.4±0.7	6.9±0.5	6.3±0.7	6.6±0.6	5.0±0.9	6.1±0.7
−0.55	6.5±0.5	6.2±0.4	6.3±0.6	5.8±0.5	5.6±0.6	4.8±0.6
−0.45	6.6±0.5	6.1±0.4	6.2±0.5	5.3±0.5	4.9±0.5	4.7±0.6
−0.35	7.0±0.5	6.0±0.4	6.1±0.5	4.6±0.5	5.2±0.5	4.4±0.5
−0.25	5.2±0.5	5.9±0.4	5.8±0.5	5.8±0.5	5.7±0.5	3.9±0.5
−0.15	6.9±0.6	5.5±0.4	6.5±0.6	6.0±0.5	4.9±0.6	4.2±0.6
−0.05	6.7±0.7	7.4±0.6	5.0±0.7	6.6±0.6	5.7±0.7	5.3±0.7
0.05	6.7±0.7	6.9±0.6	6.8±0.8	6.1±0.7	5.6±0.8	5.0±0.8
0.15	6.1±0.9	7.0±0.7	6.0±0.9	7.2±0.8	5.9±0.9	6.3±0.9
0.25	7.8±1.0	8.0±0.9	6.5±1.0	7.1±1.0	6.5±1.1	6.4±1.0
0.35	8.5±1.1	9.5±1.1	10.7±1.3	8.1±1.2	7.3±1.3	7.3±1.2
0.45	8.3±1.3	8.8±1.2	9.3±1.4	7.9±1.4	7.3±1.5	6.5±1.4
0.55	10.4±1.5	8.9±1.5	5.9±1.7	7.3±1.6	7.5±1.6	7.0±1.6
0.65	12.3±1.9	10.2±1.8	8.6±2.2	7.6±2.0	7.6±2.2	7.4±2.1

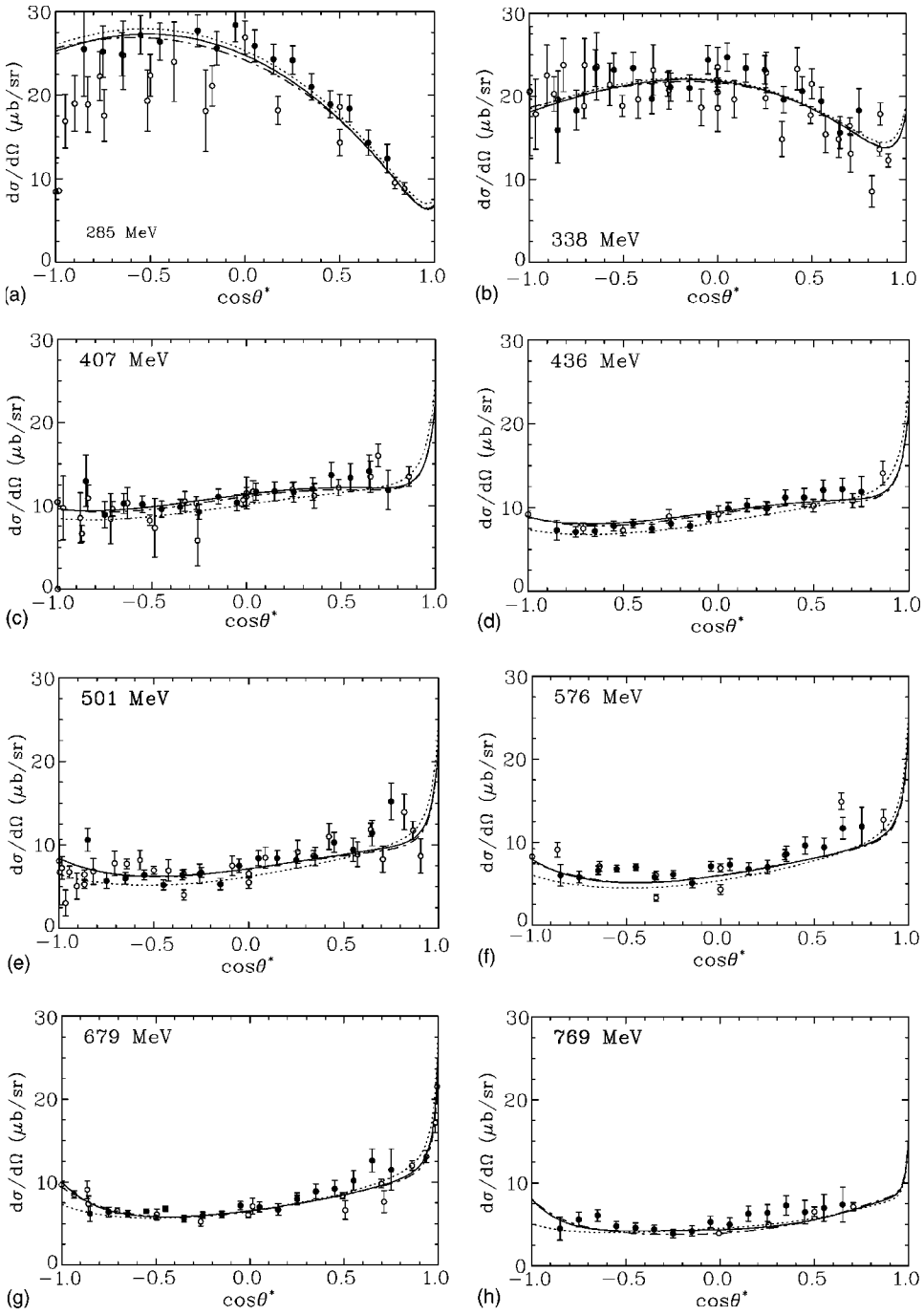

FIG. 6. Differential cross sections for $\gamma n \to \pi^- p$ at (a) 285 MeV, (b) 338 MeV, (c) 407 MeV, (d) 436 MeV, (e) 501 MeV, (f) 576 MeV, (g) 679 MeV, and (h) 769 MeV. The uncertainties are statistical only. Dashed-dotted (solid) curves correspond to the GW SAID SM02 (SH04) solution [8]. The MAID solution [13] are plotted with dashed lines. Previous measurements [28–30] are shown as open circles.

uncertainty in the CEX cross section was estimated to be about 5% which includes the addition in quadrature of the uncertainty of ~4% based on the comparison of the SAID PWA results for the CEX reaction and our measured differential cross section, an uncertainty of ~3% for central values of cos θ^* of the CEX angular distribution, and an uncertainty of ~2% in the normalization of the LH_2 data relative to the CH_2 data. The final uncertainty due to this factor varies with the magnitude of the point by point subtraction of CEX events that are misidentified as REX events; it is largest at backward and/or forward angles (depending on beam energy) where the subtraction is large (yielding an uncertainty of a few percent) and is smallest at central angles where the subtraction is small (yielding an uncertainty of a fraction of a percent). Similarly, the uncertainty in the relative normalization of the beam-related empty-target background is ~3% and has a larger effect at backward angles (several percent) than at central to forward angles (about a percent). The uncertainty in the REX differential cross section due to these factors is determined bin by bin by obtaining cross sections in the standard manner and then with each background increased by its uncertainty.

The acceptance is flat over most of the angular range with an uncertainty at the ~1% level at all but the most forward angles, where the value for the acceptance drops off rapidly and the relative uncertainty approaches a few percent. The uncertainties due to the background subtractions and acceptance corrections are angle dependent and are included in the

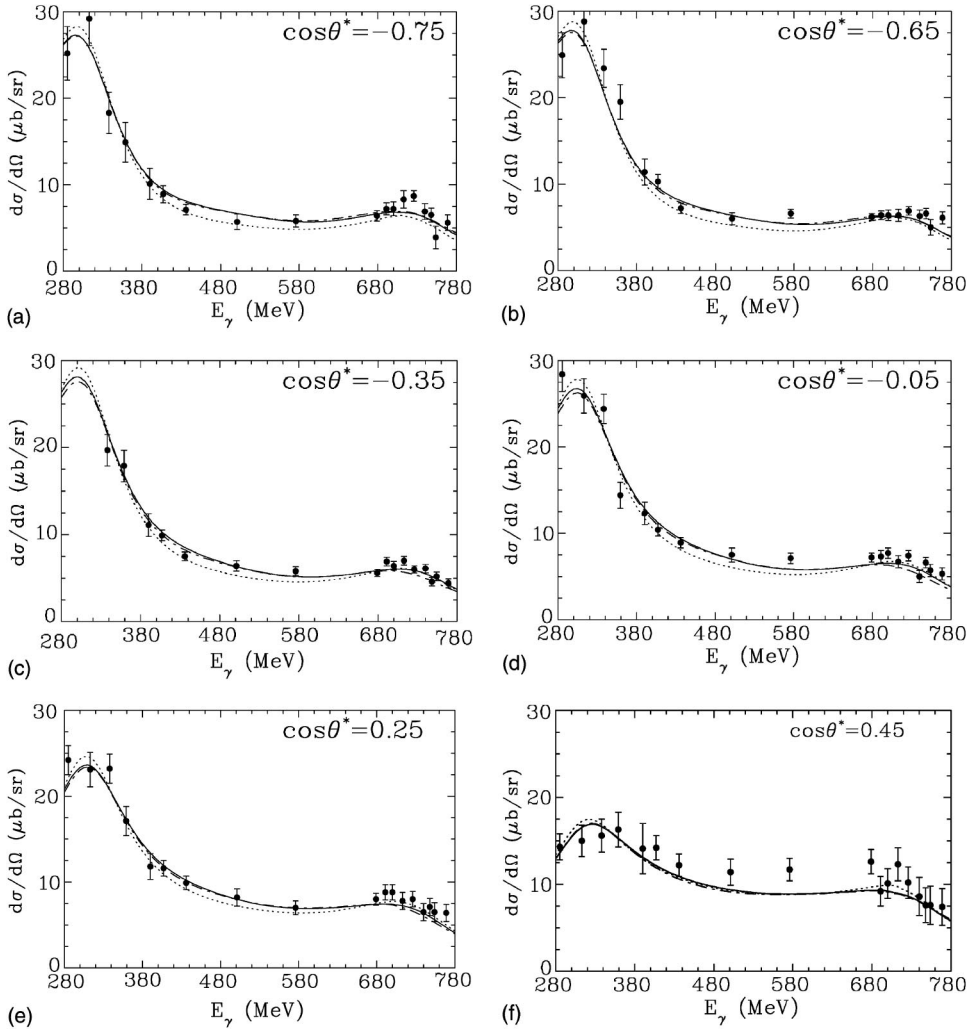

FIG. 7. Differential cross sections for $\gamma n \to \pi^- p$ at (a) $\cos\theta^* = -0.75$, (b) $\cos\theta^* = -0.65$, (c) $\cos\theta^* = -0.35$, (d) $\cos\theta^* = -0.05$, (e) $\cos\theta^* = +0.25$, and (f) $\cos\theta^* = +0.45$. Dashed-dotted (solid) curve corresponds to the GW SM02 (SH04) solution [8]. The MAID solution [13] predictions are plotted with dashed lines. The quoted uncertainties are statistical only.

uncertainties reported for the points listed in Tables II–IV.

The overall normalization uncertainty in our REX results of ~5% is mainly due to the estimated uncertainties described above for the measured CEX cross section at the central values for its angular distribution, the estimated uncertainty in the SAID CEX cross section, and uncertainty in the normalization of the LH_2 data relative to the CH_2 data. This total systematic uncertainty is not included in the figures and tables.

VI. RESULTS FOR $\gamma n \to \pi^- p$

The complete collection of the results of our experiment on $d\sigma/d\Omega(\pi^- p \to \gamma n)$ are given in the thesis by Shafi [18]. Here, we present our data converted to the inverse process. This facilitates the comparison with the numerous data sets that exist for π^+ and π^0 photoproduction on a hydrogen target. Assuming time–reversal invariance, the radiative $\pi^- p$ capture is related to π^- photoproduction on the neutron via the detailed balance relation

$$d\sigma(\gamma n \to \pi^- p) = DB\, d\sigma(\pi^- p \to \gamma n), \tag{4}$$

where $DB = \frac{1}{2}(p_\pi^*/p_\gamma^*)^2$ is the detailed balance factor, the number $\frac{1}{2}$ is the spin-factor weight for the process, and p^* is the momentum in the center of mass.

Our results in the form $d\sigma/d\Omega(\gamma n \to \pi^- p)$ are presented in Tables II–IV. A representative selection of angular distributions is shown in Fig. 6. Six examples of the excitation function at $\cos(\theta)^* = -0.75$, -0.65, -0.35, -0.05, 0.25, and 0.45 are shown in Fig. 7. The enhancement at low E_γ is due to the high-energy tail of the $\Delta(1232)$, and the small bump at large E_γ reflects the production of the $N(1520)$ and $N(1535)$. The excitation functions at all angles reveal no bump or shoulder that could be indicative of the excitation of the Roper resonance. To extract electromagnetic quantities for the Roper resonance, one should use a multipole analysis of the available pion photoproduction data. This is discussed in the next section.

The existing data come in two types: REX, as measured in our experiment, and π^--photoproduction on the deuteron. Our data are more numerous (300 points) than any of the existing REX data sets, generally agreeing with the photoproduction results that use the so-called π^-/π^+ technique for extracting the π^--photoproduction data from a deuterium target [18]. Statistical uncertainties, which include angle-dependent uncertainties due to background subtraction and acceptance corrections, generally vary from 5% to 15%, except for the most forward and backward scattering angles at low momenta where statistical uncertainties are as large as

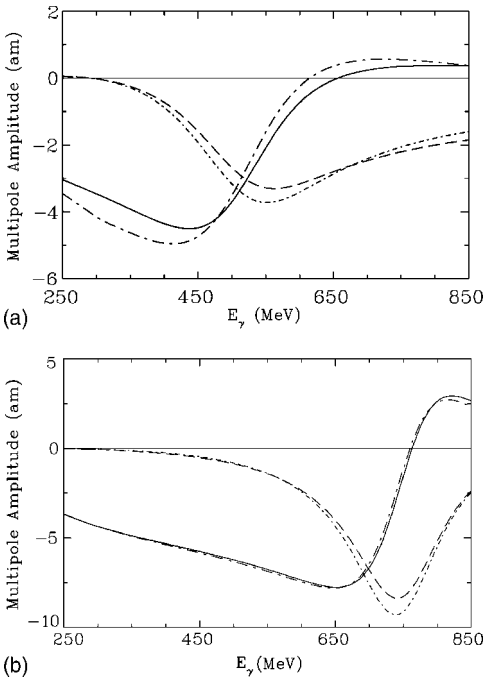

FIG. 8. Major multipoles affected by the CB data: (a) ${}_nM_{1-}^{1/2}$ and (b) ${}_nE_{2-}^{1/2}$. Solid (dashed) curves give the real (imaginary) parts of amplitudes corresponding to the GW SM02 solution [8]. The real (imaginary) parts of GW SH04 solution, are plotted as dashed-dotted (short dashed-dotted) curves. The subscript *n* denotes a neutron target.

30% for the measurements reported in this paper. The data with larger uncertainties at extreme scattering angles at each beam momentum were eliminated if either the background subtraction was very large or the acceptance was varying rapidly and the resulting angle-dependent uncertainty is greater than 30%. An overall systematic uncertainty for all energy sets of about 5% is obtained, from the sum in quadrature of all other known factors. For details, see Sec. V.

Figure 6 also displays our comparison of the predictions from the SAID PWA [8] and the MAID [13] analyses of existing data. In both analyses, large disagreements with some older bremsstrahlung measurements [28,29] are obvious, particularly at lower energies. Also plotted is the best-fit (SH04), based on a SAID analysis incorporating the current set of measurements. Both the SAID and MAID predictions give a good qualitative representation of the data. The CB data and curves are presented without any renormalization. Upon inclusion of the CB cross sections in the SH04 fit, the overall χ^2 dropped, relative to the SAID prediction, by only 25 (out of 327). We note that the structure near 700 MeV in the excitation cross sections of Fig. 7 appears sharper than predicted by SAID and MAID. The reproduction of this feature was not significantly improved in the SH04 fit.

The new CB cross sections did not result in large changes to the multipole amplitudes. Examples of multipoles on a neutron target showing typical differences are plotted in Fig. 8. However, when we include the resulting multipoles in a new three-parameter fit to extract the $A_{1/2}^n$ amplitude for the P_{11}, a change from 47 ± 5 to 49 ± 4 $(\mathrm{GeV})^{-1/2}\times10^{-3}$ is seen in the $A_{1/2}^n$ amplitude with the uncertainty in the amplitude being mainly due to the nonresonant background. This value for $A_{1/2}^n$ agrees very well with the value currently quoted by the PDG. While these analyses were performed including all published data, we did experiment with the fits by removing older data that were more than five standard deviations from the new fit. While this process decreased the reduced χ^2 to ~1.0, all other results remained the same.

VII. CONCLUSION AND DISCUSSION

We have measured a comprehensive set of differential cross sections at 18 energies for the inverse pion photoproduction reaction, $\pi^- p\to n\gamma$, over an energy range most sensitive to contributions from the Roper resonance. As is evident in Fig. 6, the existing database for this reaction was populated by a number of measurements inconsistent with the extensive SAID and MAID fits to both neutron and proton target data. Our measurements have verified the features of both the SAID and MAID analyses, however they disagree with some of the older data sets. A major accomplishment of this experiment is a substantial improvement in the π^--photoproduction data base, adding 300 new differential cross sections. Inclusion of these new data has resulted in only small changes to the SAID multipole amplitudes.

The lowest-energy differential cross section angular distribution in Fig. 6 shows that the SAID and MAID fits are in disagreement with much of the older data, but are in satisfactory agreement with the current measurement. This observation reflects the fact that neither fit is entirely model independent and individual data sets do not determine fits. Both fits use similar prescriptions to unitarize the Born-term background. In the MAID approach, resonances are added explicitly; in SAID, resonance contributions are added implicitly through a parametrization in terms of the πN T-matrix. This limitation on the form does not allow a fit to arbitrary angular variation, especially at lower energies, such as the backward dip suggested by the older data at 285 MeV as is shown very clearly in Fig. 6(a): the SAID and MAID solutions "predicted" our cross section values at 285 MeV despite the low values of the older data.

The largest differences between SAID and MAID are visible at forward and backward angles in Fig. 6, at the highest energies. Disagreements between the analyses and the new CB data are also enhanced in these regions, as we have shown in Fig. 7. It should be emphasized that the differences in the multipoles are not major and indicate that the data base is approaching an accurate representation of the REX interaction over the energy range that covers the Roper resonance, and that one can certainly rely on the SAID and MAID representations at the 10% level. We have obtained a stable value for the $A_{1/2}^n$ amplitude for the P_{11} [from 47 ± 5 to 49 ± 4 $(\mathrm{GeV})^{-1/2}\times10^{-3}$] when we include our new multipoles in a three parameter fit. This value agrees with the value quoted in Table I for the PDG. The largest uncertainty in the amplitude extraction is due to the method used to handle the nonresonant background in this fit. The remaining differences in the neutron and proton couplings for the Roper resonance in Table I are speculated to be due to the different extraction methods used by each author. These differences must be settled by further theoretical work.

On the experimental side, further improvements in the PWAs await more data in the region at and above the $N(1535)$ where the number of measurements for this reaction is small. Of particular importance in all energy regions is the need for data obtained involving polarized photons and polarized targets. Due to the closing of hadron facilities, new $\pi^- p \to \gamma n$ experiments are not in the planning and only $\gamma n \to \pi^- p$ measurements are possible at electron facilities using deuterium or helium targets. Our agreement with the existing π^- photoproduction reaction measurements lead us to believe that the photoproduction measurements are reliable despite the necessity of using a deuterium target. Plans are now in place to use the Crystal Ball and the polarized photon beam and polarized ^{1}H, ^{2}H, and ^{3}He targets at MAMI C to collect photoproduction data off the neutron in the next several years.

ACKNOWLEDGMENTS

The authors thank A. E. Kudryavtsev and A. Donnachie for useful discussions on the γn reaction. The authors acknowledge the support of the US National Science Foundation, the US Department of Energy, NSERC of Canada, the Russian Ministry of Science and Technology, the Russian Foundation of Basic Research, the Russian State Scientific-Technical Program: Fundamental Nuclear Physics, the Croatian Ministry of Science, and the George Washington University Research Enhancement Fund. The authors also thank SLAC for the loan of the Crystal Ball. The assistance of the staff of BNL and AGS is much appreciated.

[1] S. Capstick, Phys. Rev. D **46**, 2864 (1992); S. Capstick and W. Roberts, Prog. Part. Nucl. Phys. **45**, S241 (2000).
[2] S. Capstick and P. R. Page, Phys. Rev. C **66**, 065204 (2002); Z.-P. Li, V. Burkert, and Z.-J. Li, Phys. Rev. D **46**, 70 (1992).
[3] R. Bijker, F. Iachello, and A. Leviatan, Ann. Phys. (N.Y.) **236**, 69 (1994).
[4] N. Mathur, S. J. Dong, T. Draper, I. Horvath, F. X. Lee, K. F. Liu, and J. B. Zhang, submitted to Phys. Rev. D; Report No. hep-ph/0306199.
[5] R. Jaffe and F. Wilczek, Phys. Rev. Lett. **91**, 232003 (2003).
[6] C. Lovelace, CERN Report, TH-625, 1965 (unpublished).
[7] A. Donnachie, Phys. Lett. **24B**, 420 (1967).
[8] R. A. Arndt, W. J. Briscoe, I. I. Strakovsky, and R. L. Workman, Phys. Rev. C **66**, 055213 (2002).
[9] R. A. Arndt, I. I. Strakovsky, and R. L. Workman, Phys. Rev. C **53**, 430 (1996).
[10] R. L. Crawford and W. T. Morton, Nucl. Phys. **B211**, 1 (1983); Particle Data Group, Phys. Lett. B **239**, 1 (1990).
[11] R. L. Crawford, in *Proceedings of the Workshop on the Physics of Excited Nucleons (NSTAR2001), Mainz, Germany, March 7–10, 2001*, edited by D. Drechsel and L. Tiator (World Scientific, Singapore, 2001), p. 163.
[12] D. Drechsel, O. Hanstein, S. S. Kamalov, and L. Tiator, Nucl. Phys. **A645**, 145 (1999).
[13] MAID refers to the Dec. 2003 version of the MAID solution from L. Tiator, and S. Kamalov. D. Drechsel, O. Hanstein, S. S. Kamalov, and L. Tiator, Nucl. Phys. **A645**, 145 (1999).
[14] M. M. Niboh, Ph.D. thesis, Kent State University, 1997; D. M. Manley, Int. J. Mod. Phys. A **18**, 441 (2003).
[15] C. Bennhold *et al.*, in *Proceedings of the Workshop on The Physics of Excited Nucleons*, edited by D. Drechsel and L. Tiator (World Scientific, Singapore, 2001), p. 109.
[16] T. Feuster and U. Mosel, Phys. Rev. C **59**, 460 (1999).
[17] K. Hagiwara *et al.*, Phys. Rev. D **66**, 010001 (2002); http://pdg.lbl.gov
[18] A. Shafi, Ph.D. thesis, The George Washington University, 2003.
[19] A. Starostin *et al.*, The Crystal Ball Collaboration, Phys. Rev. C **64**, 055205 (2001).
[20] W. B. Tippens *et al.*, The Crystal Ball Collaboration, Phys. Rev. Lett. **87**, 192001 (2001).
[21] S. N. Prakhov *et al.*, The Crystal Ball Collaboration, Phys. Rev. C **69**, 045202 (2004).
[22] T. D. S. Stanislaus *et al.*, Nucl. Instrum. Methods Phys. Res. A **262**, 463 (2001).
[23] R. A. Arndt, W. J. Briscoe, I. I. Strakovsky, R. L. Workman, and M. M. Pavan, Phys. Rev. C **69**, 035213 (2004); the SAID database and a number of multipole analyses are available at the website: http://gwdac.phys.gwu.edu
[24] CERN Application Software Group, CERN Program Library Long Writeup W5013, 1993.
[25] W. B. Tippens *et al.*, The Crystal Ball Collaboration, Phys. Rev. D **63**, 052001 (2001).
[26] M. E. Sadler *et al.*, The Crystal Ball Collaboration, Phys. Rev. C **69**, 055206 (2004).
[27] W. S. Risk, Phys. Rev. **167**, 1249 (1968); F. Bulos *et al.*, *ibid.* **187**, 1827 (1969); J. B. Cheze *et al.*, Nucl. Phys. **B72**, 365 (1974); J. C. Comiso *et al.*, Phys. Rev. D **12**, 738 (1975); N. C. Debenham *et al.*, *ibid.* **12**, 2545 (1975); F. O. Borcherding, Ph.D. thesis, UCLA, 1982; I. V. Lopatin, Phys. At. Nucl. **65**, 236 (2002) [Yad. Fiz. **65**, 260 (2002)].
[28] J. Boucrot *et al.*, Nuovo Cimento Soc. Ital. Fis., A **18A**, 635 (1973).
[29] V. Rossi *et al.*, Nuovo Cimento Soc. Ital. Fis., A **13A**, 59 (1973).
[30] G. Neugebauer *et al.*, Phys. Rev. **119**, 1726 (1960); H. Fujii *et al.*, Phys. Rev. Lett. **26**, 1672 (1971); P. Benz *et al.*, Nucl. Phys. **B65**, 158 (1973); P. E. Scheffler *et al.*, *ibid.* **B75**, 125 (1974); J. C. Comiso *et al.*, Phys. Rev. D **12**, 719 (1975); A. J. Weiss *et al.*, Nucl. Phys. **B101**, 1 (1975); H. Fujii *et al.*, *ibid.* **B120**, 395 (1977); P. E. Argan *et al.*, Nucl. Phys. **A296**, 373 (1978); M. T. Tran *et al.*, *ibid.* **A324**, 301 (1979); G. J. Kim *et al.*, Phys. Rev. D **40**, 244 (1989).